Table 1 Parameters of the model for OH127.8 and OH104.9

	OH127.8	OH104.9
RA of centre relative to coordinate centre (arc s)	−0.11 ± 0.01	−0.12 ± 0.01
Dec. of centre relative to coordinate centre (arc s)	−0.15 ± 0.01	−0.21 ± 0.01
Position angle of rotation axis (deg)	10 ± 5	0 ± 5
Stellar velocity relative to the local standard of rest (km s^{-1})	−55.4 ± 0.2	−25.8 ± 0.2
Expansion velocity (km s^{-1})	10.9 ± 0.2	14.3 ± 0.2
Rotation velocity (km s^{-1})	0.2 ± 0.1	−0.9 ± 0.1
Shell radius (arc s)	1.53 ± 0.02	1.44 ± 0.02

These values assume that the rotation axis is perpendicular to the line of sight, because the fit is insensitive to this parameter. The quoted errors are estimated 1σ uncertainties.

For material in a uniform expanding shell, therefore, a plot of log a against log$[1-(v/v_e)^2]$ should yield a straight line with a gradient of 0.5. A plot of these quantities for some of the components of OH104.9 is shown in Fig. 4. The components to the north and south of the centre follow the uniform expanding shell model, but the components to the east, which are shown in Fig. 4, do not. Departure from a gradient of 0.5 may be caused either by an error in the assumed position of the expansion centre or by an incorrect value of v_e. Similarly, separation on the plot of high and low velocity components which are spatially coincident may be caused by an incorrect value of the central (stellar) velocity. However, even if all these parameters are allowed to vary, there is still no solution for a uniformly expanding, non-rotating shell which fits all the observed data.

We conclude that the kinematics of the components depart from a simple expanding shell model not only because of small-scale turbulence as mentioned above, but also because of a large scale non-radial motion. The simplest explanation of the non-radial motion is that the shell is rotating about the star as well as expanding from it. The kinematics of a rotating, expanding, thin shell are easily modelled and we have used a computer least squares program to fit such a model to the data on OH127.8 and OH104.9, resulting in the parameters given in Table 1. In each case, there is excellent agreement between the model and the data, and the r.m.s. error in velocity is ~0.3 km s^{-1}, which is less than half our velocity resolution of 0.8 km s^{-1}. The model for OH127.8 shows no significant rotation, but the shell around OH104.9 is rotating with an equatorial speed of 0.9 km s^{-1}.

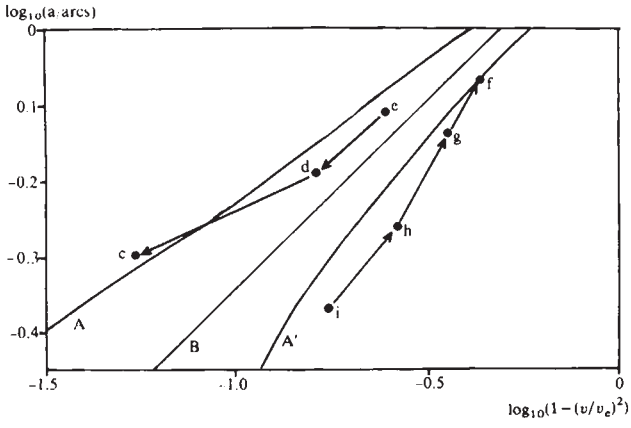

Fig. 4 A plot of $\log_{10} a$ against $\log_{10}(1-(v/v_e)^2)$ for components at position angle 90° (see text). Line B is the curve expected from a simple expanding shell model. Lines A and A′ are the curves expected from a rotating expanding shell. ●, The observed data, and the arrows connecting them are in the direction of increasing velocity. Despite the large scatter in the data points, they show clearly the bifurcation expected from a rotating expanding shell. Small letters against data points correspond to the maps in Fig. 3.

The angular momentum of the shell may be derived either from rotation of the star or from the orbital angular momentum of a binary companion. The former explanation implies a high rate of angular momentum loss from the star, leading us to favour the second explanation. A plausible model would separate the binary companion from its primary by ~10^{15} cm, implying an orbital period of the order of hundreds of years. The current position of the companion, which may destroy the conditions for maser emission, may lie to the west of the source, where there is no detectable OH maser emission. These models are developed and discussed in more detail in ref. 10.

The evaluation of the mass loss rate from long period variable stars is of great importance in understanding stellar evolution. By assuming[3] a molecular hydrogen number density of 2×10^4 cm^{-3}, we derive a mass loss rate of $8\times10^{-5}\,M_\odot$ yr^{-1} for OH127.8 and $5\times10^{-5}\,M_\odot$ yr^{-1} for OH104.9. Such high mass loss rates agree well with the IR properties of OH/IR stars[11], although they imply a short lifetime for a star in this state.

We have produced further evidence for the evidence of a simple expanding shell around OH127.8, and have shown that OH104.9 possesses a shell which is rotating as well as expanding, and may be a member of a binary system. It is clearly necessary to extend these results to other sources, and such work is in progress.

Received 13 May; accepted 2 July 1982.

1. Davies, J. G., Anderson, B. & Morison, I. *Nature* **288**, 64–66 (1980).
2. Norris, R. P., Booth, R. S. & Diamond, P. J. *Mon. Not. R. astr. Soc.* (in the press).
3. Booth, R. S., Kus, A. J., Norris, R. P. & Porter, N. D. *Nature* **290**, 382–384 (1981).
4. Cornwell, T. J. & Wilkinson, P. N. *Mon. Not. R. astr. Soc.* **196**, 1067–1086 (1981).
5. Hogbom, J. A. *Astr. Astrophys. Suppl.* **15**, 417–426 (1974).
6. Jewell, P. R., Webber, J. C. & Snyder, L. E. *Astrophys. J. Lett.* **242**, L29–L31 (1980).
7. Herman, J. & Habing, H. in *Proc. Workshop on Physical Processes in Red Giants*, Erice (1980).
8. Norris, R. P. & Booth, R. S. *Mon. Not. R. astr. Soc.* **195**, 213–226 (1981).
9. Baud, B. *Astrophys. J. Lett.* **250**, L79–L83 (1981).
10. Diamond, P. J., Norris, R. P., Booth, R. S. Withington, S. W. & Rowland, P. R. 1982 (in preparation).
11. Werner, M. W. *et al. Astrophys. J.* **239**, 540–548 (1980).

Ion nucleation—a potential source for stratospheric aerosols

F. Arnold

Max-Planck-Institut für Kernphysik, Postfach 103 980, 6900 Heidelberg, FRG

The stratospheric aerosol layer is of considerable interest for its potential influence, at least temporarily, on the Earth's radiation budget and climate[1]. While the nature of the aerosol is now reasonably well established the mechanisms leading to the formation of new particles are poorly understood[2–4]. It is thought that the aerosols are formed by heterogeneous heteromolecular condensation involving sulphuric acid and water vapour and pre-existing condensation nuclei (CN) of tropospheric or meteoric origin. The resulting supercooled solution droplets which are composed of ~75% (by mass) H_2SO_4 and 25% H_2O undergo condensational and coagulational growth and are ultimately removed from the stratosphere by gravitational sedimentation. CN-formation in the stratosphere by homogeneous or ion nucleation (IN) has largely been found to be inefficient[2–6]. I have now investigated the role of ion nucleation in stratosphere aerosol formation in the light of recent progress in both the areas of stratospheric ion composition[7] and sulphuric acid vapour[8–10] measurements. In constrast to previous conclusions ion nucleation is found to be a potential source for stratospheric aerosols.

Ion nucleation involves growth of ions by association of gas molecules to a critical size at which the resulting molecular cluster is stable against evaporational destruction after neutralization of its net charge by ion–ion recombination. In

0028-0836/82/360134—04$01.00

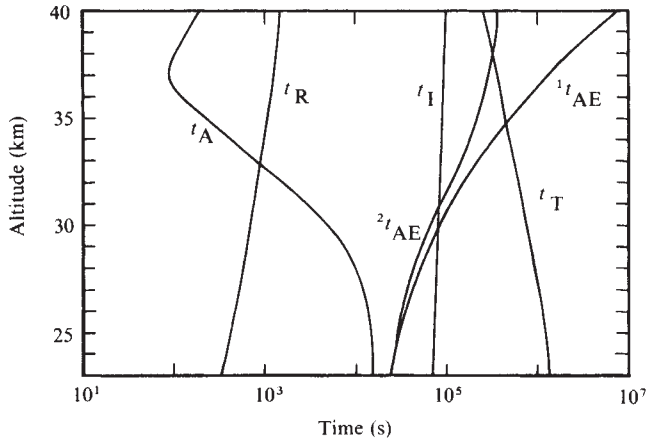

Fig. 1 Typical time scales for ion growth (t_A), ion–ion recombination (t_R), H_2SO_4 attachment to ions (t_I and aerosols (t_{AE}) and vertical turbulent transport (t_T). For t_A two cases, H_2SO_4–H_2O aerosols ($^1t_{AE}$) and, in addition to these, meteoric smoke particles ($^2t_{AE}$) (7% recondensation of meteor vapour) are given[17]. For details see text. For t_R evaluation measured α and $n_\pm$ values were taken.

stratospheric conditions only molecular clusters containing H_2SO_4 and H_2O molecules can form CN. Consequently only ions containing H_2SO_4 and H_2O molecules can be involved in IN. It has been found recently[7] from baloon-borne composition measurements of stratospheric negative ions that the most abundant ion species above 27 km are $H_2SO_4\,(H_2SO_4)_n(H_2O)_m$ and that these already develop properties similar to H_2SO_4–H_2O solution droplets for $n \geq 3$. The time scale for addition of an H_2SO_4 molecule to an ion is $t_A = (k[H_2SO_4])^{-1}$ where k is a phenomenological binary rate coefficient for H_2SO_4 association being typically of the order of 10^{-9} cm^3 s^{-1} in the conditions considered[11,12] and $[H_2SO_4]$ is the concentration of H_2SO_4-vapour molecules.

The ion lifetime compared with ion–ion recombination is $t_R = (\alpha n_\pm)^{-1}$ where α is the effective ion–ion recombination coefficient and $n_\pm$ is the total charged particle concentration.

The abundance ratio $R_{n,n+1}$ for ions containing $n+1$ and n H_2SO_4 molecules is obtained from a simple steady state treatment

$$R_{n+1,n} = (1 + t_A/t_R)^{-1} \quad (1)$$

accordingly one obtains the approximation

$$R_{n_c,0} = (1 + t_A/t_R)^{-n_c} \quad (2)$$

where n_c is the number of H_2SO_4 molecules contained in an ion cluster which also remain stable against evaporational destruction after neutralization.

Thus the ion nucleation rate is

$$J = Q(1 + t_A/t_R)^{-n_c} \quad (3)$$

where Q is the galactic cosmic ray ionization rate, being of the order of 10 cm^{-3} s^{-1} in the middle stratosphere[13].

The critical quantity n_c may be set equal to the number of H_2SO_4 molecules contained in an electrically neutral drop which is just stable and whose size may be obtained from the Kelvin expression[14]. The latter relates the droplet radius r_c to the supersaturation ratio $S = p/p_0$ where p and p_0 are the partial and equilibrium saturation pressures for sulphuric acid vapour. For $S \leq 6$, n_c becomes larger than ~10 and increases steeply as S increases. This is consistent with laboratory studies[15] of IN suggesting that IN becomes efficient for $S \geq 4$–6. However, usually in these studies $t_A \ll t_R$, in contrast to the stratospheric situation.

Typical t_A and t_R values are shown in Fig. 1. Measured α and $n_\pm$ were taken (ref. 16, and D. Smith, personal communication) and k was set equal to 10^{-9} cm^3 s^{-1}. Value for H_2SO_4] were taken from recent measurements[8–10] (Fig. 2) where it was found that $[H_2SO_4]$ below ~27 km is similar to the lower limit curve predicted by the theoretical model case of Turco *et al.*[17] which neglects H_2SO_4 re-evaporation from the aerosol. Above ~35 km, $[H_2SO_4]$ is similar to the upper limit curve CHA 75) predicted by a purely photochemical diffusive model[18] which neglects H_2SO_4 condensation. In the intermediate altitude range (27–35 km) $[H_2SO_4]$ is similar to $[H_2SO_4]_s$, the expected equilibrium saturation pressure for H_2SO_4 over the aerosol[9,10].

Thus it appears that $S < 1$ above ~35 km, $S = 1$ between ~27 and 35 km and $S > 1$ below ~27 km. That implies that aerosols are unstable above ~35 km and that IN can occur only at heights below ~27 km. Since $[H_2SO_4]_s$ increases strongly as temperature increases, the $[H_2SO_4]_s$ curves are different for winter and summer due to seasonal temperature changes. Corresponding $[H_2SO_4]_s$ curves for winter (45 W) and summer (45 S) and 45° latitude are also shown in Fig. 2.

Ion nucleation rates J calculated from equation (3) for average winter and summer temperatures at 45° latitute are shown in Fig. 3. Here the curve T80 (Fig. 2) was taken as a lower limit to $[H_2SO_4]$.

Generally the calculated J values increase as height increases and decrease abruptly above a certain height where S becomes smaller than ~10 and where consequently n_c becomes large. This is due to the large t_A/t_R ratios in this height region. Maximum J values of about 3×10^{-3} cm^3 s^{-1} (winter) and 5×10^{-4} cm^3 s^{-1} (summer) are reached around 29 km and 24 km respectively. Corresponding column IN rates J_c are $\sim 9.3 \times 10^2$ cm^{-2} s^{-1} (winter) and 1.6×10^2 cm^{-2} s^{-1} (summer). By comparison, the globally averaged J_c required to maintain the stratospheric aerosol layer is only of the order of 0.01 cm^{-2} s^{-1}.

Thus IN apparently has the potential to form more CN than required to seed the stratospheric aerosol layer.

However, a large fraction of the newly formed CN may become removed before they can grow a new aerosol solution droplet. Loss processes may involve mostly CN attachment to aerosols. The lifetime of a gas molecule (molecular weight 29) against collision with aerosols t_{AE} is given in Fig. 1. Below 30 km it is of the order of only 10^4–10^5 s. In comparison, the time scale for adding an H_2SO_4-gas molecule to a CN having a radius of 10^{-7} cm is of the order of 10^4 s. Thus a newly formed CN can pick up a few more H_2SO_4-vapour molecules before it collides with an aerosol solution droplet. This is particularly true as the CN lifetime against collision with aerosols should be much larger than t_{AE} due to the large CN mass.

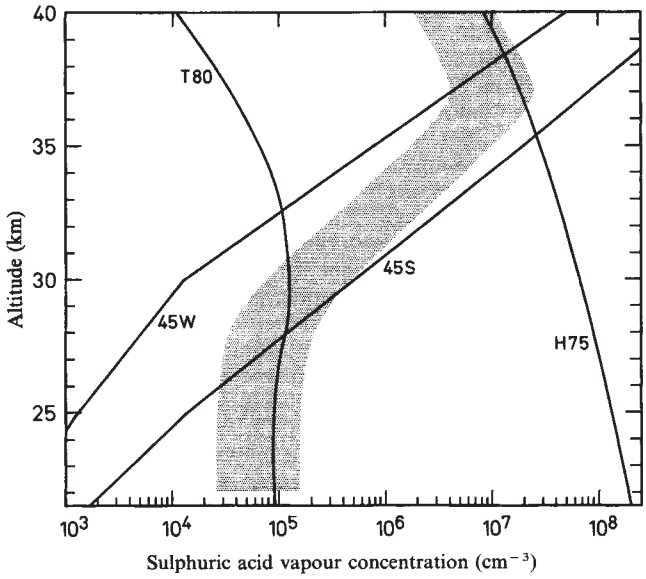

Fig. 2 Sulphuric acid vapour concentrations. Measured values[8–10] are indicated by the shaded area. Extreme cases as obtained from theoretical model calculations are indicated by H75 (all sulphuric acid in the gas phase[17]) and T80 (no re-evaporation of sulphuric acid vapour[16]) for average winter and summer temperatures at 45° latitude are also shown.

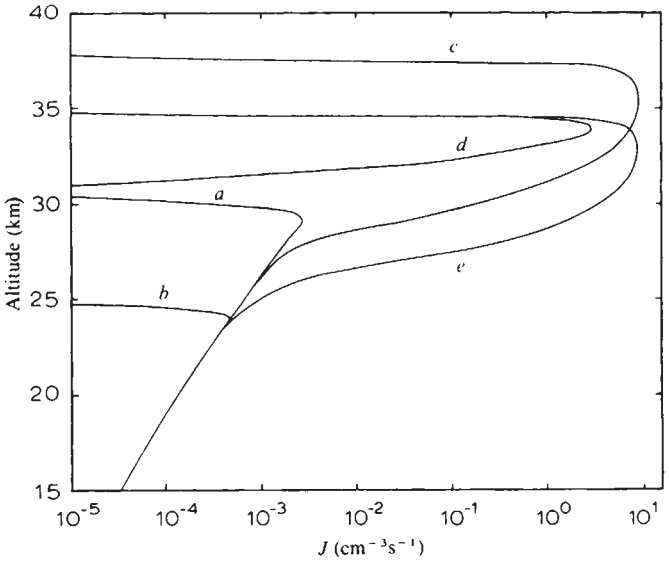

Fig. 3 Calculated ion nucleation rates J: *a*, average winter temperatures (T_w); *b*, average summer temperatures (T_s); *c*, cooling from T_s to T_w; *d*, cooling from T_s+5 to T_s; *e*, cooling from T_s+10 to T_s.

Assuming a CN lifetime against attachment to aerosols of 10^5 s and a yearly averaged J of the order of $10^{-3}\,cm^{-3}\,s^{-1}$ around 25–30 km one obtains an average CN concentration [CN] of the order of $100\,cm^{-3}$ for the 25–30-km region and $10\,cm^{-3}$ for 20 km.

Measured[19] [CN] are about $1–100\,cm^{-3}$ (25–30 km) and $1–10\,cm^{-3}$ (20 km) and compare reasonably well with the above model predictions for altitudes below about 25–30 km.

However, no CN formation occurs above 25–30 km in the conditions considered and therefore CN must be transported, mostly by turbulent diffusion, to this height range. The time scale for vertical turbulent diffusion t_T (per kilometre) is given in Fig. 1, being $\sim10^5$–10^6 s (1–10 days). Thus it is much larger than the CN lifetime against collision with aerosols, which implies that little vertical CN transport should occur below ~35 km. Consequently, CN observed above 25–30 km can hardly be explained by the above IN model.

In the stratosphere, however, dramatic departures from a condensation–evaporation equilibrium for sulphuric acid can occur. These should be induced by short-term temperature changes which are quite common, particularly at lattitudes >45° during local winter[20]. An example of temperature changes at 35 km in Fig. 4 shows measured temperatures along with average summer (S), spring–autumn (SA) and winter (W) values. Typical amplitudes and time scales are about 5–10° and one to a few days respectively in winter; occasionally, dramatic temperature enhancements, 'sudden stratospheric warmings', occur[20] during which temperatures may even exceed summer values. These events are thought[2] to arise mostly from large amplitude planetary waves pumping heat energy from the tropical troposphere and stratosphere to the polar regions. Thus, the radiative imbalance in the atmosphere arising from the smaller amount of solar radiation absorbed at high latitudes is compensated through adiabatic processes.

As the temperature increases, $[H_2SO_4]_s$ increases (by about a factor of 10 per 10° (refs 22, 23). Eventually the entire H_2SO_4–H_2O aerosol may evaporate, depending on the maximum temperature reached, in which case $[H_2SO_4]$ would be equal to curve H75 (Fig. 2). As the temperature falls again, sulphuric acid vapour may become highly supersaturated with respect to the condensed H_2SO_4–H_2O phase.

The time scale for H_2SO_4-vapour recondensation on aerosols is larger than t_{AE} (Fig. 1), being ~1 day around 30 km. This implies that high supersaturations may persist for at least 1 day.

A typical case for a major winter warming would be a temperature rise to average summer values and a subsequent cooling to average winter values which implies a maximum S of ~3 (Fig. 2). Corresponding J values are shown in Fig. 3 (curve *c*). Around 35 km they become comparable to Q ($10\,cm^{-3}\,s^{-1}$) and fall off steeply above and less steeply below this height. The thickness of the IN layer is ~5 km. The fall-off towards larger heights is mostly due to a decrease of S causing a steep increase of n_c. The fall-off towards smaller heights is mostly due to the decrease of $[H_2SO_4]$ causing an increase of t_A/t_R.

Summer IN events for temperature increases of 5° and 10° and subsequent coolings to average summer values are also shown in Fig. 3 (curves *d* and *e*). These IN layers peak around 34 and 33 km respectively and are ~1.5 and 5 km thick respectively.

For curves *c*, *d* and *e* maximum J values are sufficiently large to allow for a rapid build-up of a limiting [CN], being of the order of $10^5\,cm^{-3}$ within <1 day. For $[CN]\geq10^5\,cm^{-3}$ the lifetime of a CN against mutual CN coagulation becomes ≤1 day. For $[CN]=10^5\,cm^{-3}$ the lifetime of an H_2SO_4-vapour molecule against attachment to a CN is of the order of 10^4–10^5 s. Consequently the supersaturated H_2SO_4 vapour should become consumed by condensation onto the newly formed CN within a day or less, leading to an average aerosol corresponding to only 10^3–10^4 H_2SO_4 molecules or ~4–8×10^{-7} cm in radius.

In the days after their formation the CN undergo further mutual CN coagulation until [CN] has fallen to a level of $\sim10^3$–$10^4\,cm^{-3}$, at which the time scale for coagulation becomes weeks to months. At these time scales vertical turbulent diffusion becomes efficient, having a time scale t_T of the order of a few days per kilometre. Vertical turbulent diffusion leads to a broadening of the CN layer and a further decrease of the peak [CN] value.

Upward diffusion carried the CN into a region where $S<1$ leading to CN evaporation. Downward diffusion carries CN into a region of large S where they are safe from evaporational destruction by subsequent warming events.

It appears then that IN due to warming–cooling events is an efficient CN source at heights around 27–37 km. It may give rise to average [CN] values of the order of 10^3–$10^4\,cm^{-3}$, corresponding to average CN sizes of 1.6×10^{-6} cm and 8×10^{7} cm respectively.

The column IN rates J_c corresponding to curves *c*, *d* and *e* (Fig. 3) are $\sim4\times10^7\,cm^{-2}\,s^{-1}$, $1\times10^7\,cm^{-2}\,s^{-1}$ and $4\times10^7\,cm^{-2}\,s^{-1}$.

The column IN production for long-lived CN only (lifetime >1 day) are $\sim6\times10^{10}\,cm^{-2}$, $1\times10^{10}\,cm^{-2}$ and $6\times10^{10}\,cm^{-2}$. In comparison, the persistent IN source existing below

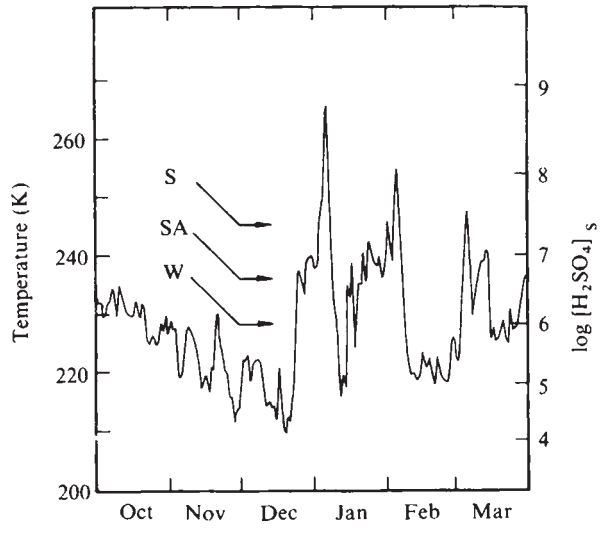

Fig. 4 Stratospheric temperatures (E. Pantzke, personal communication) as measured at 35 km altitude over Berlin (52°N, 14°E) during the winter 1975–76. Corresponding saturation concentrations for sulphuric acid vapour and average winter–, spring–autumn- and summer temperatures[24] are also given.

25–30 km leads to a column production of $\sim 2 \times 10^{10}$ cm^{-2} for an entire year.

Thus the warming–cooling events contribute substantially to, or even dominate, the overall CN production. Regionally and during certain periods of time they give rise to large CN concentrations in the 27–37 km range.

Note that there is a possible influence of solar activity on the CN production by IN. Galactic cosmic radiation, the only important source of ionization in the undisturbed stratosphere, is partly shielded by the interplanetary magnetic field which gives rise to an anticorrelation of Q and solar activity. Typically Q values by about a factor of 4 over a solar sunspot cycle at middle latitudes. Since $n_{\pm} = (Q/\alpha)^{1/2}$, t_R varies by a factor of about 2. The t_R curve shown in Fig. 1 and used for the above calculations corresponds to solar sunspot maximum conditions (large t_R).

For solar sunspot minimum, t_R is smaller by a factor of 2, leading to smaller IN rates, particularly in conditions where $t_A/t_R \gg 1$. For example, the maximum value of curve a (Fig. 3) would be smaller for solar sunspot minimum conditions by about a factor of 10.

Thus the global CN production by IN may be substantially smaller during conditions of low solar activity. As a consequence the aerosol size distribution may shift towards larger sizes as fewer CN compete for the available sulphuric acid. As a change of the aerosol size distribution may affect the radiation properties of the stratospheric aerosol layer, solar activity changes may modulate the possible influence of the stratospheric aerosol layer on the Earth's radiation budget and climate.

Finally possibilities for observational tests of the ion nucleation hypothesis will be discussed. Observable quantities are [CN], [H_2SO_4] and the ion composition. Concerning [CN] the IN model seems to be in harmony with measurements. In particular the CN layer recently detected by Hofmann and Rosen[19] around 30–35 km is readily explained and its major features are reasonably well reproduced by the IN model.

It seems, however, that predicted [CN] values are larger than observed ones. As far as [H_2SO_4] and ion composition measurements are concerned only few data exist. It would be desirable to carry out coordinated measurements of [CN], [H_2SO_4] and ion composition during a major winter warming–cooling event. During the early phase of the cooling large S values and very complex ion clusters should occur while large [CN] values should persist for days after the onset of the cooling.

Note that the above model calculations of IN are only rough approximations and that extensive model calculations of stratospheric IN should be carried out.

I thank D. J. Hofmann, P. Hamill, K. Labitzke and B. Naujukat for helpful discussions, and E. Pantzke for providing stratospheric temperature data.

Received 3 March; accepted 8 June 1982.

1. Pollack, J. B. *et al. J. geophys. Res.* **81**, 1971 (1976).
2. Cadle, R. D. & Grams, G. W. *Rev. Geophys. Space Phys.* **13**, 475 (1975).
3. Toon, O. B. & Farlow, N. H. *A. Rev. Earth planet. Sci.* **9**, 19 (1981).
4. Castleman, A. W. Jr *A. Rev. Earth planet. Sci.* **9**, 227 (1981).
5. Hamill, P., Turco, R. P., Toon, O. B., Kiang, C. S. & Whitten, R. C. *J. Aerosol Sci.* (submitted).
6. Mohnen, V. A. *Proc. 4th Conf. on CIAP* (US Department of Transportation, 1975).
7. Arnold, F., Viggiano, A. & Schlager, H. *Nature* **297**, 371–376 (1982).
8. Arnold, F. & Fabian, R. *Nature* **283**, 55 (1980).
9. Arnold, F., Fabian, R. & Joos, W. *Geophys. Res. Lett.* **8**, 293 (1981).
11. Arnold, F., Fabian, R., Ferguson, E. E. & Joos, W. *Planet. Space Sci.* **29**, 195 (19812).
12. Viggiano, A. A., Perry, R. A., Albritton, D. L., Ferguson, E. E. & Fehsenfeld, F. C. *J. geophys. Res.* **85**, 4551 (1980).
13. Webber, W. *J. Geophys. Res.* **67**, 5091 (1962).
14. Thomfor, G. & Volmer, M. *Ann. Phys.* **5**, 109 (1939).
15. Castleman, A. W. Jr *Adv. Colloid Interface Sci.* **10**, 73 (1979).
16. Gringel, W., Hofmann, D. J. & Rosen, J. M. *Rep. No AP-47* (University of Wyoming, Laramie, 1978).
17. Turco, R. P., Toon, O. B., Hamill, P. & Whitten, R. C. *J. geophys. Res.* **86**, 113 (1981).
18. Harker, A. B. *J. geophys. Res.* **80**, 3399 (1975).
19. Hofmann, D. M. & Rosen, J. M. *Nature* **297**, 120 (1982).
20. Labitzke, K. *J. geophys. Res.* **86**, 9665 (1981).
21. Schoeberl, M. R. *Rev. Geophys. Space Phys.* **16**, 521 (1978).
22. Ayers, G. F., Gillett, R. W. & Gras, J. L. *Geophys. Res. Lett.* **7**, 433 (1980).
23. Rödel, W. *J. Aerosol Sci.* **10**, 375 (1979).
24. *U.S. Standard Atmosphere Supplements* (US Government Printing Office, Washington DC 1966).

Ozone vertical distribution and total content using a ground-based active remote sensing technique

J. Pelon & G. Megie

Service d'Aéronomie du CNRS, BP 3, 91370-Verrieres-Le-Buisson, France

The evaluation of possible perturbations of anthropogenic origin on the Earth environment has become increasingly important with the development of industrial and agricultural activities. Among these the depletion of the ozone layer under the influence of chemically active minor constituents produced by anthropogenic sources is still under question, thus emphasizing the importance of ozone monitoring in the atmosphere. Beside classical systems, such as the Dobson spectrometer and Brewer or ECC sondes, new techniques of ozone monitoring are being developed which include passive IR and microwave spectrometry and active IR and UV laser soundings[1]. They should soon allow complementary routine measurements. We have previously described[2] the UV lidar system set up at the Observatoire de Haute Provence (44° N, 6° E) in the south of France and the methodology of the differential absorption laser technique (DIAL) which provide routine measurements of the ozone vertical distribution from the ground up to 25 km. We report here the first active ground-based measurements of the ozone distribution at higher altitudes up to 40 km and of the total ozone content using the same system.

Attempts to measure ozone number density above its maximum using a ground-based UV system are complicated because the extinction of the laser emitted light is high due to the absorption in the lower altitude layers. Furthermore the rapid decrease in ozone number density above 28 km requires very rapidly increasing acquisition times for the measurement[2]. To overcome these major problems, a different wavelengths pair B (305.8–310.8 nm) was chosen to probe the upper levels (13–38 km) as compared with the one A (288.8–294.5 nm) previously adopted for the lower altitude range. These wavelengths choices minimize the interferences by other absorbing gases (SO_2–NO_2) and by aerosol particles and optimize the signal-to-noise ratio[2]. Whereas ozone distribution measurements in the boundary layer can be performed using the DIAL method[3], we have restricted our measurements to the altitude range above 3 km to avoid any problem related to geometrical effects and to the large dynamic of the backscattered signals in the first few kilometres. Compared with the previously reported measurements[2], a factor of 5 reduction in the acquisition time has been obtained by increasing the receiving telescope diameter from 36 to 80 cm. The parameters of the lidar system are listed in Table 1. Adopted values for the ozone absorption cross-sections are those of Inn and Tanaka[4] corrected for temperature dependence as given by Vigroux[5].

Figure 1 represents two lidar measured ozone profiles as obtained on 1 and 2 December 1981 at 00 h UT. The acquisition time for each profile is 90 min. The vertical resolution varies between 360 m in the troposphere, 1.2 km at 25 km and 3.6 km

Table 1 Parameters of the lidar system

Emitted wavelengths		
A pair	$\lambda_1 = 288.80$ nm	$\lambda_2 = 294.50$ nm
B pair	$\lambda_1 = 305.80$ nm	$\lambda_2 = 310.80$ nm
Spectral width	$\Delta\lambda < 5$ pm	
Emitted energy	$E = 40$ mJ–10 Hz	
Divergence	< 0.5 mrd	
Telescope	ϕ 80 cm	
Field of view	0.7 mrad	

0028-0836/82/360137—03$01.00